Nanotechnology **19** (2008) 085715 (8pp) doi:10.1088/0957-4484/19/8/085715

Small-angle neutron scattering measurement of silicon nanoparticle size

Jonghoon Choi[1,2], **Shih-Huang Tung**[1,3], **Nam Sun Wang**[1] **and Vytas Reipa**[2]

[1] Department of Chemical and Biomolecular Engineering, University of Maryland, College Park, MD 20742, USA
[2] Biochemical Science Division, National Institute of Standards and Technology, Gaithersburg, MD 20899, USA

E-mail: vytas@nist.gov

Received 10 August 2007, in final form 31 October 2007
Published 4 February 2008
Online at stacks.iop.org/Nano/19/085715

Abstract

We have determined the particle size distribution profiles of octane-terminated silicon nanoparticle suspensions, produced using the sonication of electrochemically etched Si wafers. Small-angle neutron scattering data was analyzed separately in high ($0.4\ \text{nm}^{-1} < q < 3.0\ \text{nm}^{-1}$) and low ($q < 0.4\ \text{nm}^{-1}$) scattering vector ranges. Data in the high q range is consistent with the log-normal distribution of isolated spherical particles with median diameter $d = 3 \pm 0.2$ nm.

Particle sizes were also indirectly assessed from photoluminescence and optical transmission spectroscopy using the size/bandgap relation: $E_g = 3.44d^{-0.5}$, where E_g is in eV and d in nm. Both measurements were consistent with the particle size distribution profiles, estimated from ANS data fitting and TEM image analysis.

A subpopulation of larger, irregular shape structures in the size range 10–50 nm was also indicated by neutron scattering in the low q range and HRTEM images. However, further studies are warranted to explain a relationship between the slope of scattering intensity versus scattering vector dependence in the intermediate scattering vector range ($0.4\ \text{nm}^{-1} < q < 1.0\ \text{nm}^{-1}$) and the role of non-geometrical Si nanoparticle characteristics (mutual interaction forces, surface termination, etc).

1. Introduction

Semiconductor nanocrystals or quantum dots have size-dependent physical properties due to confinement of charge carriers to particle dimensions when they are comparable to the Bohr radius of an exciton. Bulk silicon is a rather inefficient light emitter due to the indirect bandgap electronic structure that requires lattice vibration quanta (phonon) to balance electron momentum during the interband transition. Such three-particle (electron, photon and phonon) collisions have very low probability and the emission efficiency of bulk silicon at room temperature is very low. Fortunately, momentum requirements are relaxed in 1–5 nm dia Si crystals as a result of quantum confinement effects and bright photoluminescence in the UV/vis range is observed.

Photoluminescent Si nanocrystals (SNs) along with C-and SiC-based nanoparticles are considered more bio-inert than metal chalcogenide-based quantum dots [1] and may lead to the development of biocompatible and smaller probes [2–4]. Also, Si nanostructures are actively pursued for LED, display, solar energy conversion and sensing applications [5]. Current SN production procedures [3, 6–9] typically do not allow for the fine control of particle size.

A published method [2, 3, 10] to make H-terminated SNs consists of anodic Si wafer etching with subsequent breakup of the porous film in an ultrasound bath. Resulting H-termination provides a useful platform for further surface chemical derivatization. Such a procedure is typically used to prepare highly photoluminescent SNs; however, a rather polydisperse mixture is produced after sonication, leading to inhomogeneous broadening of the photoluminescence spectrum as a result of distributed bandgap energies and

[3] Present address: Department of Materials Science and Engineering, University of California, Berkeley, CA 94720, USA.

varying degrees of surface passivation. It has been speculated that sonication does not produce individual Si nanoparticles, but rather nanocrystalline domains that may be trapped in micron-sized silicon pieces [11]. From a technological point of view, a homogeneous nanoparticle size mixture would be highly desirable, as it narrows the optical bandwidth. Moreover, a reliable measurement of the nanoparticle size distribution profile is essential in separating the role of dimensional, structural and chemical factors that determine particle optical properties [12]. Nanoparticle size also controls their uptake by cells and their final localization inside the cell [13, 14].

Previously, we have described a new method of SN size reduction, using photo-assisted dissolution [3]. This method exploits nanoparticle dissolution rate variation with particle size, and has demonstrated narrowing of size polydispersity. In this study, we present our small-angle neutron scattering (SANS) measurements on a suspension of very small (below 5 nm in diameter) photoluminescent Si particles, produced by ultrasonic crumbling of the porous Si film. Crystal size distributions, obtained from SANS data, were compared with the measurements from several other methods: high resolution transmission electron microscopy (HRTEM), photoluminescence (PL) and optical transmission spectroscopy (OTS).

Conventional particle size measurements, based on light scattering, rely heavily on the accurate knowledge of the particle index of refraction that happens to be size-dependent in quantum dots [15] and at present is quite poorly defined.

SANS is regularly used to characterize structures in the nanometer range [16–24]. Although often SANS is applied in polymer structural studies, the utility of the method was recently demonstrated for metal nanoparticles in alloys [18], nanodroplet aerosols [19], surface-modified nanorods [20] and laser synthesized silicon nanopowders [22–24]. Botti *et al* reported an excellent agreement between transmission electron microscopy (TEM) results and SANS data for the relatively large Si particles (>5 nm in diameter) [23, 24]. However, an insufficient TEM resolution could not confirm the presence of the smallest particles (<5 nm), which were indicated by SANS data [24]. Furthermore, their method of Si nanoparticle production is known to generate particle agglomerates that shift the resulting size distribution towards larger crystals [25].

We have estimated the mean diameter of Si nanoparticles in a deuterated cyclohexane colloidal suspension by employing Guinier and Porod approximations [17]. Our experimental conditions favor the production of small, single nanometer range objects that could be detected in the presence of larger, aggregated Si particles. Using the scattering intensity versus scattering vector plot fitted to a polydisperse set of spherical shaped particles, we calculate the log-normal Si nanoparticle diameter distribution profiles. These profiles were judged against the independent particle size assessment from HRTEM, absorbance and photoluminescence. SANS demonstrated a rather narrow spherical nanoparticle distribution centered on the diameter $d = 3.0 \pm 0.2$ nm and a subpopulation of larger structures with a mean diameter $d = 18.3 \pm 0.5$ nm. Photoluminescence spectra are consistent with the size–bandgap relation, described in [26], if we account for the inhomogeneous broadening due to size polydispersity.

2. Experimental section

2.1. Nanoparticle preparation

Silicon wafers were electrochemically etched in a HF:H_2O:ethanol (1:1:2, volume ratio) mixture by following the lateral etching procedure [27]. Polished wafers (⟨111⟩ oriented, 0.001–0.01 Ω cm, As doped) were purchased from Virginia Semiconductor, Inc., Fredericksburg VA[4]. Anodic etching was performed in a polycarbonate cell that accommodates a 100 mm dia Si wafer placed between two Pt wire mesh cathodes. Electrical contact was provided to the top edge of the vertically mounted wafer and electrolyte was slowly pumped into the cell, hence providing a moving electrolyte boundary. Total etch time typically was about 4 h per 100 mm dia wafer at 120 mA constant current, supplied by a galvanostat (Model 363, EG&G Inc., Princeton, NJ). Following anodic etching, the wafer is washed several times in deionized water, methanol (HPLC grade, Mallinckrodt Chemicals, Phillipsburg, NJ) and blow-dried in a stream of nitrogen. Dry wafers displayed an intense orange-red luminescence under 365 nm UV lamp excitation. Next, Si wafers were subjected to 2 h of sonication in a deaerated pure 1-octene (Sigma-Aldrich, St. Louis, MO) under vigorous N_2 purging. The resulting suspension displayed broad-band PL in the orange/red spectral range under UV (365 nm) excitation.

2.2. Surface functionalization

Following sonication, 20 ml of the Si nanoparticle suspension was placed in a quartz container that was mounted inside the UV reactor (model RMR-600, Rayonet, Branford, CT) and exposed to 254 nm light for 30 min in an N_2 atmosphere. Silicon nanoparticles acquire octane termination as a result of the hydrosilylation reaction and are stabilized against air oxidation. Next, the sample was filtered with a 0.2 μm syringe filter and dried in vacuum. Dry Si nanoparticles were redispersed in deuterated cyclohexane for SANS measurements.

2.3. Small-angle neutron scattering (SANS)

SANS measurements were performed on the NG-7 (30 m) beamline at the National Institute of Standards and Technology (NIST) in Gaithersburg, MD [28]. Neutrons with a wavelength of 0.6 nm were selected. A wide range of wavevectors from 0.03–5.0 nm^{-1} were probed at three sample–detector distances of 1, 4 and 13.25 m. This range of wavevectors corresponds to structural sizes ranging from 1 to 200 nm. Silicon nanoparticle samples were suspended in deuterated cyclohexane (Cambridge Isotope Laboratories Inc., Andover,

[4] Certain commercial equipment, instruments, materials or companies are identified in this paper to specify adequately the experimental procedure. Such identification does not imply recommendation nor endorsement by the National Institute of Standards and Technology, nor does it imply that the materials or equipment identified are the best available for the purpose.

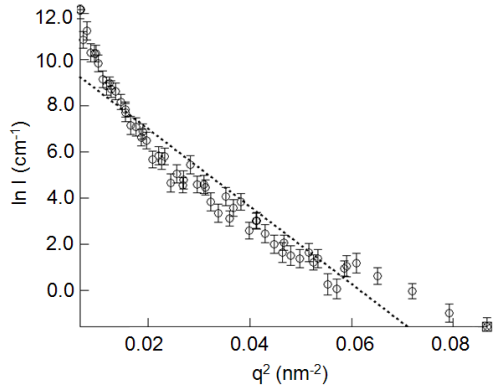

Figure 1. Guinier fit of SANS spectrum of the octane-functionalized silicon nanocrystal suspension in the low q ($0.04\ \text{nm}^{-1} < q < 0.4\ \text{nm}^{-1}$) region.

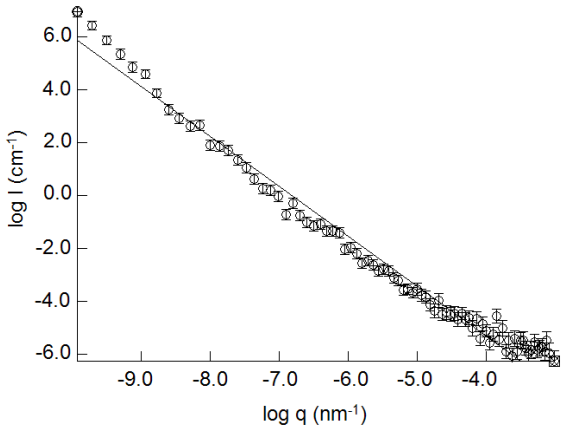

Figure 2. SANS spectrum of the octane-functionalized Si nanoparticle suspension in the high q range ($1.0\ \text{nm}^{-1} < q < 5.0\ \text{nm}^{-1}$) and a linear fit to the Porod approximation (see text).

MA) and studied in 1 mm quartz cells at 25 °C. Scattering spectra were corrected and located on an absolute scale based on calibration standards provided by NIST. Data is shown as radially averaged intensity I versus wavevector $q = (4\pi/\lambda)\sin(\theta/2)$, where λ is the wavelength of the incident neutrons and θ is the scattering angle.

2.4. SANS data analysis

SANS data was processed with IGOR software (version 5.0, Wavemetrics, OR) [29]. In a first step, Guinier and Porod approximations are utilized to obtain mean particle diameter and volume fraction, thus reducing the number of free variables for the model fit. Next, a fit to experimental scattering intensity data was used to calculate the particle number density based on the volume fraction and polydisperse particle volume.

2.5. High resolution transmission electron microscopy (HRTEM)

HRTEM images were acquired on a JEM2100F (JEOL, Tokyo, Japan) microscope at the University of Maryland, College Park. A drop of SN suspension in toluene was deposited on a TEM carbon grid (Tedpella, Redding, CA) and allowed to evaporate in the ambient atmosphere.

2.6. Photoluminescence (PL) and optical transmittance spectroscopy (OTS)

Silicon nanoparticle suspension photoluminescence was measured in a 1 cm quartz cell with a SLM LM800 spectrofluorimeter (SLM Inc., Rochester, NY) set at 360 nm excitation. UV–vis transmittance of the octane-covered SN suspension in toluene was recorded with an Ocean Optics (Dunedin, FL) Chem2000 fiber optic spectrophotometer. A first-order derivative of the transmission spectrum was calculated using GRAMS/AI software (ver. 7.0, Thermo Electron Co., Boston, MA). A steady-state nanoparticle photoluminescence spectrum ($\lambda_{\text{exc}} = 365$ nm) was acquired with an SLM LM800 spectrofluorimeter.

3. Results and discussion

Our primary objective is to measure Si particle size distribution in the quantum confinement range that includes nanoparticles with diameters less than 5 nm, as only in this size range do Si crystals display bright visible photoluminescence [10].

3.1. Measurement of the mean particle diameter

We have used the Guinier approximation for spherical particles to obtain the average diameter of nanoparticles (equation (1)):

$$\ln\left(\frac{\mathrm{d}\Sigma}{\mathrm{d}\Omega}\right) \approx \ln\left[(\overline{\rho}_{\text{bd}} - \overline{\rho}_{\text{bm}})^2 C_{\text{p}} \frac{1}{6}\pi d^3\right] - \frac{q^2 d^2}{20} \qquad (1)$$

where $\frac{\mathrm{d}\Sigma}{\mathrm{d}\Omega}$ is the scattering cross section, $\overline{\rho}_{\text{bd}} - \overline{\rho}_{\text{bm}}$—a contrast factor, defined as the difference between the mean neutron scattering length densities of the particle and solvent materials, C_{p}—particle volume fraction, d—particle mean diameter and q—the scattering vector, $q = \frac{4\pi \sin(\phi/2)}{\lambda}$, with ϕ as a scattering angle and λ as the scattered radiation wavelength in the medium.

Based on equation (1), the mean particle diameter can be estimated from the slope of the scattering cross-section logarithm against the square of the scattering vector ($\ln(\frac{\mathrm{d}\Sigma}{\mathrm{d}\Omega})$ versus q^2, figure 1).

We have obtained the mean nanoparticle diameter, $d = 18.3 \pm 0.5$ nm, from the Guinier fit to SANS data, as shown in figure 1. Next, we have estimated particle volume fraction $C_{\text{p}} = 3.0\ e^{-3}$ from the y intercept of the linear fit. However, the above mean particle diameter, calculated using the Guinier approximation, may not represent the scattering data in the high q range ($q > 0.4\ \text{nm}^{-1}$) and thus excludes the smallest particles due to the limitations of the Guinier law in the high q range. Indeed, our data meet the Guinier applicability condition ($q \cdot R_{\text{g}} < 1$, where R_{g}—particle gyration radius) [17, 30] only for the scattering vector values less than $1.0\ \text{nm}^{-1}$ and, consequently, for the high q range, we

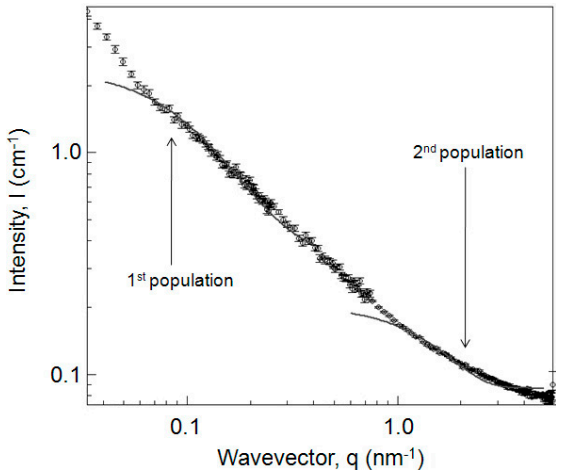

Figure 3. SANS data fits to the log-normal polydisperse spherical form factor model in the low and high q ranges.

have utilized the asymptotic Porod law (equation (2)):

$$\ln\left(\frac{\mathrm{d}\Sigma}{\mathrm{d}\Omega}\right) \approx \ln\left[\frac{12\pi C_{\mathrm{p}}\left(\overline{\rho}_{\mathrm{bd}} - \overline{\rho}_{\mathrm{bm}}\right)^2}{d}\right] - 4\ln q. \qquad (2)$$

The linear data fit (figure 2) to the Porod approximation in the range $q > \sim 1.0$ nm^{-1} returned a slope, equal to -4.1 ± 0.2, that represents a smooth interface between the scattering domains in a multiphase system [30] and justifies the application of the Porod approximation [17]. A spherical particle diameter d was obtained from the y intercept (-4.8 ± 0.1) of the ($\mathrm{d}\Sigma/\mathrm{d}\Omega$) versus q plot as indicated in equation (2). Using C_{p} ($3.0e^{-3}$) and scattering contrast values, estimated earlier from the low q interval (Guinier model fit), the mean particle diameter $d \sim 3.0$ nm was calculated from the y intercept. A similar approach was used earlier by Häußler *et al* and Lin *et al* [31–33] in studies of hydrated tricalciumsilicate and Pt nanoparticles. We have tested the robustness of our fit by varying the C_{p} within 10% of the mean value. As a result, the mean particle diameter d deviated about 11% from its mean value ($d = 3.0$ nm).

3.2. Measurement of the particle size distribution

For a dilute solution of non-interacting scattering objects, the SANS intensity $I(q)$ can be represented in terms of the form factor $P(q)$ of the scattering object. The form factor $P(q)$ for a log-normal distribution of spheres is expressed as [34]

$$P(q) = \left(\frac{\pi}{6}\right)^2 N_0 \Delta\rho^2 \int_0^\infty f(d) d^6 [F(q \cdot d)]^2 \,\mathrm{d}(d) \qquad (3)$$

where d—diameter; $f(d) = \frac{\sqrt{2}}{\sigma d\sqrt{\pi}} \exp[-\frac{1}{2\sigma^2}(\ln(\frac{d}{2}) - \mu)^2]$—number density; $F(x) = \frac{[\sin(x) - x\cos(x)]}{x^3}$—spherical scattering amplitude; N_0—the total number of particles per unit volume; $\Delta\rho$—differential scattering length density; σ—the particle polydispersity; and $\mu = \ln(d_{\mathrm{med}}/2)$—median particle diameter. The justification for using the log-normal size distribution was available from the TEM image analysis (see figure 5).

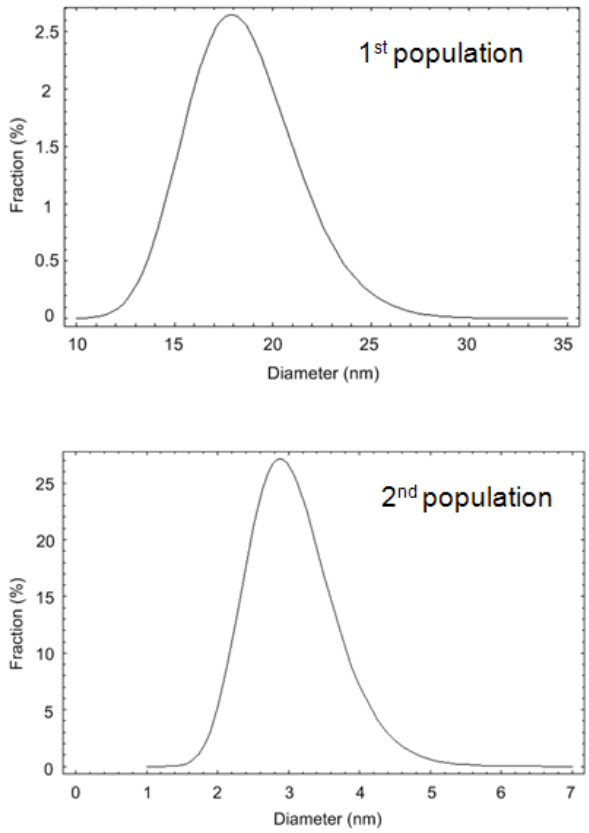

Figure 4. Size distributions from the model approximations and SANS data fits at the low (0.04 nm$^{-1} < q < 0.4$ nm^{-1}) and high (0.4 nm$^{-1} < q < 3$ nm^{-1}) q ranges.

Most of the required parameters (μ, volume fraction, scattering densities and background) were already estimated from the Guinier and Porod approximations for low and high q ranges, and the last unknown parameter—the polydispersity function σ—was calculated from the model fit of the entire SANS dataset using the NIST SANS analysis package for polydisperse spheres, assuming the log-normal size distribution (figure 3).

Typically, both the form and structure factors for a monodisperse system are oscillatory functions with clearly expressed minima and maxima. However, they are progressively smeared with increasing polydispersity or when the instrumental conditions are not perfect (e.g. due to the polychromatic neutron source). This offers a way to determine size polydispersity using a missing first minimum of the structure factor. However, our particle suspension concentration was very low ($C_{\mathrm{p}} = 3.0e^{-3}$). Therefore the structure factor was not included in the fitting.

Using the earlier estimated mean particle diameter values ($d_1 = 18.3$ nm and $d_2 = 3.0$ nm) as input parameters, we have calculated particle size distributions for both size populations (figure 4).

The scattering profile from spherical particles typically shows an intensity plateau at the lowest q ($q \cdot R_{\mathrm{g}} < 1$, where R_{g} is the gyration radius) [35, 36]: however, we did not observe such a feature at $q < 0.1$ nm^{-1} (figure 3). This suggests that a spherical particle model may not adequately represent

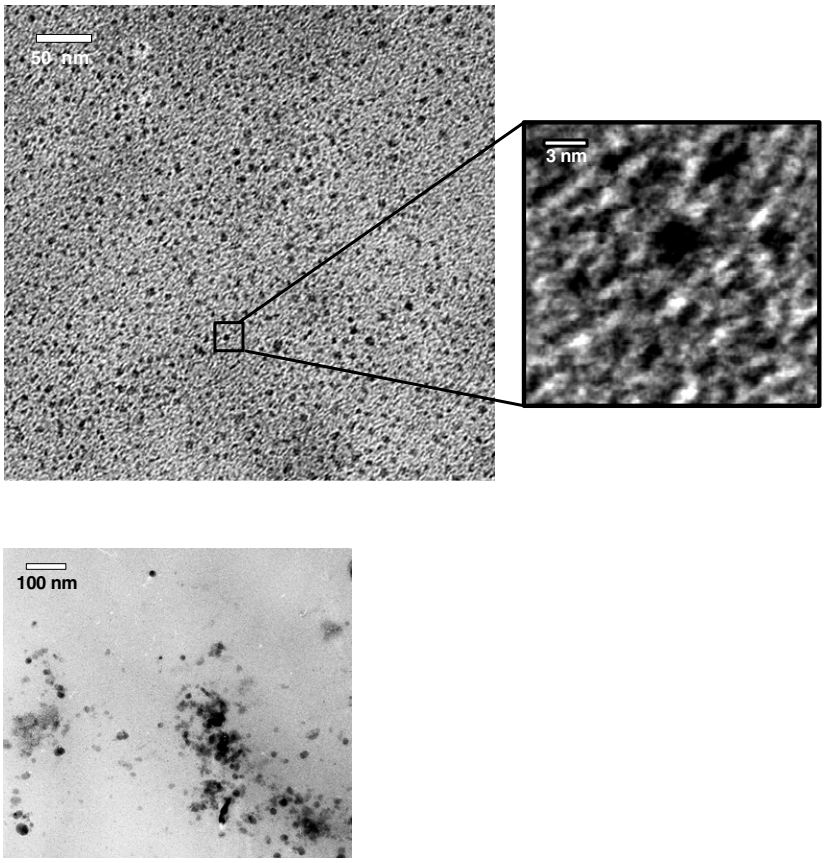

Figure 5. HRTEM images, recorded with octane-derivatized silicon nanoparticles.

our suspension scattering in the larger length scales. A more realistic model should include the cylindrical shaped particles, as they are known to elevate neutron scattering at low q [29, 37] Indeed, as evidenced by the HRTEM image (figure 5), our sample contains a subpopulation of large, aggregated, irregular shape structures (lower panel in figure 5) that are created when the columnar structure of the nanoporous silicon film breaks during the sonication [38]. In addition, the particle gyration radius average is weighted toward larger particles in the polydisperse mixture. Due to the higher scattering intensity of larger particles, their contribution to the overall SANS signal would be boosted even at lesser concentrations [17, 39].

We have assumed that, at high q, the slope of the I versus q curve equal to -4 indicates spherical dimensionality. However, the scattering from fractal objects often contributes to the slope (i.e. dimensionality) of I versus q at high q range [31–33, 39], and the contribution of the fractal structures in the single nanometer range to the scattering signal cannot be unambiguously excluded from consideration. Since our experimental conditions conform to the dilute particulate system [39], the data was analyzed without further modeling of the fractal structures.

3.3. Particle size analysis using HRTEM, absorbance and photoluminescence measurements

In addition to SANS, Si particle samples were analyzed using HRTEM, absorbance and photoluminescence measurements. Taken separately, each method has limitations and application domains, and therefore a multi-technique nanoparticle size characterization allows us to reduce uncertainties in size–property correlations and offers independent cross-validation.

HRTEM provides a direct way to assess particle dimensions from the suspension residue that was imaged following solvent evaporation (figure 5). The small amount of octane-covered SNs were dispersed on a carbon TEM grid, dried in air and placed in the vacuum chamber. Most microscope images corroborate a rather narrow distribution of spherical shape particles with diameters in the range from 2 to 5 nm: however, larger structures were visible in some areas (lower panel of figure 5).

A histogram of the SN diameters was obtained using the image analysis toolkit from Matlab (The Mathworks, Natick, MA) (figure 6) and exhibits a normal-like particle size distribution centered at 3.1 nm. Since the lower detection limit of TEM is around 2 nm, a histogram may be slightly biased toward the larger particles. An overlay of SANS particle size measurement results in the high-q (figure 4, 2nd population) and HRTEM histogram shows an excellent correlation between these two datasets (figure 6), considering that TEM has sensitivity limitation for sizes below $\sim$2 nm.

Photoluminescence spectra of SNs can be used to assess the particle size based on the quantum dot size–bandgap relationship. Previously PL profiles have been measured on various sized SN preparations (for a summary see [40])

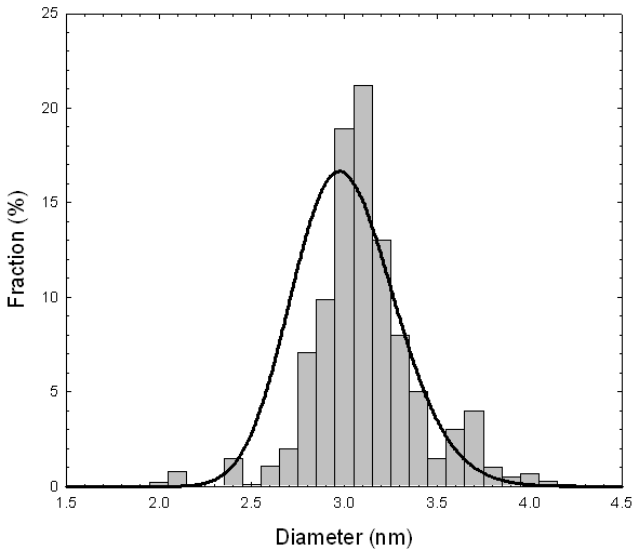

Figure 6. Si nanoparticle diameter histogram, calculated from the high resolution TEM image (total particle count $n = 962$)—gray bars, and SANS log-normal polydisperse sphere model fit in the high q range ($0.4\ \mathrm{nm}^{-1} < q < 3.0\ \mathrm{nm}^{-1}$)—solid line.

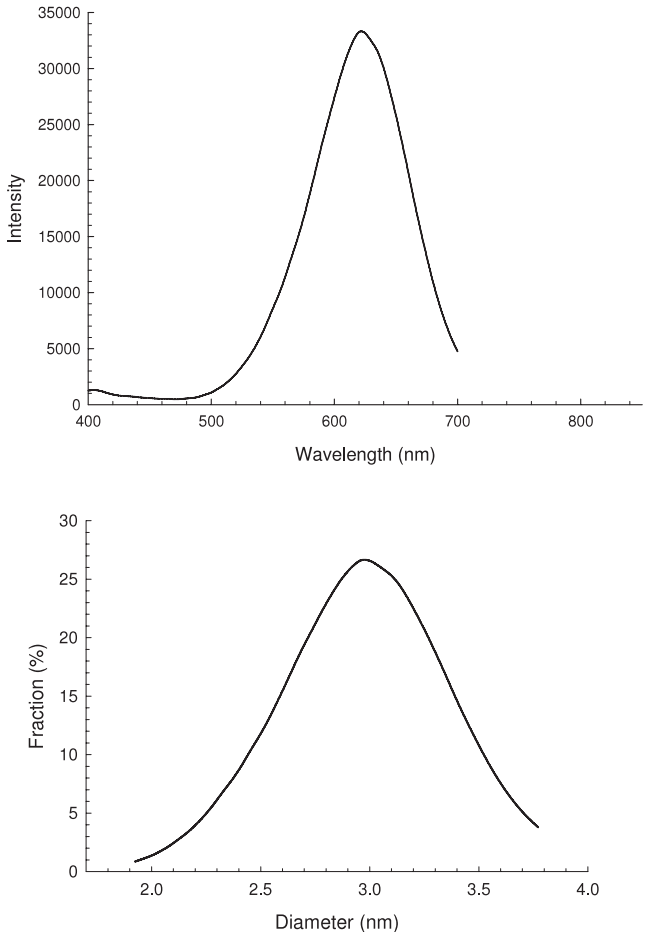

Figure 7. Photoluminescence spectrum of the octane-terminated Si nanoparticle suspension. $\lambda_{exc} = 360$ nm (upper panel) and particle size distribution, calculated assuming a single-particle PL emission FWHM = 0.1 eV and size/ bandgap relation: $E_g = 3.44d^{-0.5}$, where E_g is in eV and d in nm (lower panel).

and a power law relation between the bandgap (E_g) and spherical particle diameter (d) was established, [26], $E_g = 3.44d^{-0.5}$, where E_g is in eV and d in nm. Given that the PL bandwidth at the single Si nanoparticle level (FWHM) is ∼100–150 meV [41], and assuming comparable PL quantum yield for the different sized particles, a broad (fwhm ∼ 0.4 eV) PL profile in figure 7 (upper panel) with peak energy at ∼1.98 eV can be transformed into a particle size distribution function with a median diameter equal to 2.99 nm (lower panel of figure 7). Although this number is rather close to the median size values obtained from SANS and TEM measurements, taken separately, the PL spectrum does not offer a reliable way to measure the nanoparticle size distribution as only 'bright' entities can contribute to the overall signal. Consequently, a sizable fraction of 'dark' particles can escape detection by PL measurement, e.g. due to the defective surface structure [42].

Optical transmission measurements can also lead to a particle size distribution estimate, given the bandgap/size dependence and assuming that particles would be transparent to photons with lesser energies than their bandgap E_g. As was demonstrated by Fonseca *et al* [43], the particle size distribution function is calculated using the first derivative of the particle transmission spectrum, and approximating the particle absorbance with a step function. This measurement accounts for all particles that affect optical transmission, regardless of their photoluminescence. However, an elastic scattering by large particles may interfere with transmission derivative computation. Figure 8 shows the transmission spectrum of our octane-terminated silicon nanoparticle suspension (upper panel) and a size distribution function (lower panel), calculated following the procedure, outlined in [43], and using the size–bandgap relation proposed by [26]. Median particle diameter $d \sim 2.95 \pm 0.2$ nm reproduces accurately the peak position, obtained previously from SANS, HRTEM and PL measurements (see figures 4, 6 and 7). However, the size distribution profile is sharper and contains a tail toward larger particles (figure 8). It is to be expected that the optical transmission approximation at the bandgap by a step function [43] cannot adequately describe the nanoparticle absorbance behavior; therefore, a more elaborate dependence may be necessary to account for the absorbance variation at the band edge.

4. Conclusions

We have determined the particle size distribution profiles for the octane-terminated silicon nanoparticle suspensions, produced using the sonication of an electrochemically etched Si wafer. Small-angle neutron scattering (SANS) data was analyzed separately in the high q ($0.4\ \mathrm{nm}^{-1} < q < 3.0\ \mathrm{nm}^{-1}$) and low q ($q < 0.4\ \mathrm{nm}^{-1}$) scattering vector ranges. Data in the high q range is consistent with the log-normal distribution of isolated spherical particles with median diameter $d = 3 \pm 0.2$ nm. A subpopulation of larger, irregularly shaped structures in the size range from 10 to 50 nm was indicated by neutron scattering in the low q range and high resolution

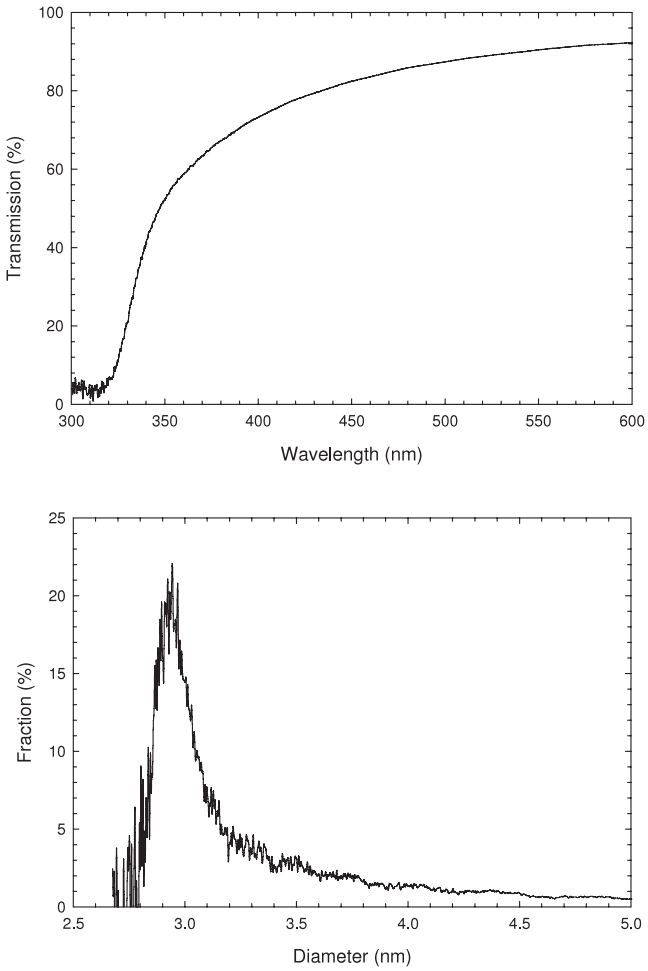

Figure 8. Si particle suspension optical transmission spectrum (upper panel) and calculated size distribution function (bottom panel).

transmission electron microscopy (HRTEM) images. Particle size was also indirectly obtained by use of photoluminescence and optical transmission spectroscopy, based on the empirical size/bandgap relation: $E_g = 3.44d^{-0.5}$, where the energy gap—E_g is in eV and diameter—d in nm. Both results are consistent with the particle size distribution profiles estimated from SANS data fitting and TEM image analysis.

Further studies are needed to explain the relationship between the slope obtained from the plot of scattering intensity versus scattering vector in the intermediate scattering vector range ($0.4\ \text{nm}^{-1} < q < 1.0\ \text{nm}^{-1}$) and the role of the non-geometrical Si nanoparticles' characteristics (mutual interaction forces, surface termination, etc). SANS measurements at higher nanoparticle concentrations together with the modeling of the fractal structures in the upper q range may provide more detailed information about the dimensionality of the smallest particles.

Acknowledgments

This work utilized facilities supported in part by the National Science Foundation under Agreement No. DMR-0454672. We thank Professor Srinivasa R Raghavan of the Department of Chemical and Biomolecular Engineering at the University of Maryland for valuable discussions and help with SANS measurements. We also acknowledge the support of the National Institute of Standards and Technology, US Department of Commerce, in providing the neutron research facilities used in this work.

References

[1] Reboredo F A and Galli G 2005 Theory of alkyl-terminated silicon quantum dots *J. Phys. Chem.* B **109** 1072–8
[2] Wang L, Reipa V and Blasic J 2004 Silicon nanoparticles as a luminescent label to DNA *Bioconjug. Chem.* **15** 409–12
[3] Choi J, Wang N S and Reipa V 2007 Photoassisted tuning of silicon nanocrystal photoluminescence *Langmuir* **23** 3388–94
[4] Ding Z, Quinn M B, Haram A K, Pell L E, Korgel B A and Bard A L 2002 Electrochemistry and electrogenerated chemiluminescence from silicon nanocrystal quantum dots *Science* **296** 1293–7
[5] Canham L 2000 Gaining light from silicon *Nature* **408** 411–2
[6] Bley R A and Kauzlarich S M 1996 A low-temperature solution phase route for the synthesis of silicon nanoclusters *J. Am. Chem. Soc.* **118** 12461–2
[7] Heath J R 1992 A liquid–solution-phase synthesis of crystalline silicon *Science* **258** 1131–3
[8] Aihara S, Ishii R, Fukuhara M, Kamata N, Terunuma D, Hirano Y, Saito N, Aramata M and Kashimura S 2001 Electroreductive synthesis and optical characterization of silicon nanoparticles *J. Non-Cryst. Solids* **296** 135–8
[9] Hua F, Swihart M T and Ruckenstein E 2005 Efficient surface grafting of luminescent silicon quantum dots by photoinitiated hydrosilylation *Langmuir* **21** 6054–62
[10] Yamani Z, Ashhab S, Nayfeh A, Thompson W H and Nayfeh M 1998 Red to green rainbow photoluminescence from unoxidized silicon nanocrystallites *J. Appl. Phys.* **83** 3929–31
[11] Veinot J G C 2006 Synthesis, surface functionalization, and properties of freestanding silicon nanocrystals *Chem. Commun.* 4160–8
[12] Adam S, Talapin D V, Borchert H, Lobo A, McGinley C, de Castro A R B, Haase M, Weller H and Möller T 2005 The effects of nanocrystal surface structure on the luminescence properties: photoemission study of HF-etched InP nanocrystals *J. Chem. Phys.* **123** 1–10
[13] Hardman R 2006 A toxicologic review of quantum dots: toxicity depends on physicochemical and environmental factors *Environ. Health Perspect.* **114** 165–72
[14] Chithrani B D, Ghazani A A and Chan W C W 2006 Determining the size and shape dependence of gold nanoparticle uptake into mammalian cells *Nano Lett.* **6** 662–8
[15] Theiss W and Hilbrich S 1997 Refractive index of porous silicon *Properties of Porous Silicon* ed L Canham (Malvern: INSPEC) pp 223–8
Koshida N 1997 *Dielectric Constant of Porous Silicon* (Malvern: INSPEC) pp 234–7
[16] Melnichenko Y B and Wignall G D 2007 Small-angle neutron scattering in materials science: recent practical applications *J. Appl. Phys.* **102** 02110101–24
[17] Sköld K and Price D L 1987 *Methods of Experimental Physics: Neutron Scattering* vol 23 (Florida: Academic) part C
[18] Strunz P, Mukherji D, Pigozzi G, Gilles R, Geue T and Pranzas K 2007 Characterization of core–shell nanoparticles by small angle neutron scattering *Appl. Phys.* A **88** 277–84
[19] Wyslouzil B E, Cheung J L, Wilemski G and Strey R 1997 Small angle neutron scattering from nanodroplet aerosols *Phys. Rev. Lett.* **79** 431–4

[20] Rajh T, Thurnauer M C, Thiyagarajan P and Tiede D M 1999 Structural characterization of self-organized TiO_2 nanoclusters studied by small angle neutron scattering *J. Phys. Chem.* B **103** 2172–7
[21] Pozzo D C and Walker L M 2007 Small-angle neutron scattering of silica nanoparticles template in PEO-PPO-PEO cubic crystals *Colloids Surf.* A **294** 117–29
[22] Botti S, Cicognani G, Coppola R, Lapp A and Magnani M 2000 Particle size and optical performances of photoluminescent laser synthesized Si nanopowders *Physica* B 276–8
Botti S, Cicognani G, Coppola R, Lapp A and Magnani M 2000 *Physica* B 860–1
[23] Botti S, Coppola R, Gourbilleau F, May R P, Rizk R and Valli M 2002 SANS and TEM investigation of laser-synthesized photoluminescent Si nanoparticles *Appl. Phys.* A **74** s1230–2
[24] Botti S, Coppola R, May R P and Valli M 2003 Photoluminescence properties and size distribution in laser synthesized Si nanopowders for optoelectronic devices *J. Appl. Crystallogr.* **36** 632–5
[25] Li X, He Y, Talukdar S S and Swihart M T 2003 Process for preparing macroscopic quantities of brightly photoluminescent silicon nanoparticles with emission spanning the visible spectrum *Langmuir* **19** 8490–6
[26] Belomoin G, Therrien J, Smith A, Rao S, Twesten R, Chaieb S, Nayfeh M H, Wagner L and Mitas L 2002 Observation of a magic discrete family of ultrabright Si nanoparticles *Appl. Phys. Lett.* **80** 841–3
[27] Jung K H, Shih S, Hsieh T Y, Kwong D L and Lin T L 1991 Intense photoluminescence from laterally anodized porous Si *Appl. Phys. Lett.* **59** 3264–6
[28] Glinka C J, Barker J G, Hammouda B, Krueger S, Moyer J J and Orts W J 1998 The 30 m small-angle neutron scattering instruments at the National Institute of Standards and Technology *J. Appl. Crystallogr.* **31** 430–45
[29] Kline S R 2006 Reduction and analysis of SANS and USANS data using IGOR Pro *J. Appl. Crystallogr.* **39** 895–900
[30] Hammouda B 1995 A tutorial on small-angle neutron scattering from polymers *NIST Pub* (June) 60
[31] Häußler F, Palzer S, Eckart A and Hoell A 2002 Microstructural SANS—studies of hydrating tricalciumsilicate (C3S) *Appl. Phys.* A **74** (Suppl.) S1124–7
[32] Häußler F, Palzer S and Eckart A 2000 Nanostructural investigations on carbonation of hydrating tricalcium silicate by small angle neutron scattering *Lacer* **5** 181–96
[33] Lin J M, Lin T L, Jeng U S, Zhong Y J, Yeh C T and Chen T Y 2007 Fractal aggregates of the Pt nanoparticles synthesized by the polyol process and poly(N-vinyl-2-pyrrolidone) reduction *J. Appl. Crystallogr.* **40** s540–3
[34] http://www.ncnr.nist.gov/programs/sans/data/data_red.html
[35] Hubbard F P Jr, Santonicola G, Kaler E W and Abbott N L 2005 Small-angle neutron scattering from mixtures of sodium dodecyl sulfate and a cationic, bolaform surfactant containing azobenzene *Langmuir* **21** 6131–6
[36] Brasher L L and Kaler E W 1996 A small-angle neutron scattering (SANS) contrast variation investigation of aggregate composition in cationic surfactant mixtures *Langmuir* **12** 6270–6
[37] Norman A I, Fei Y, Ho D L and Greer S C 2007 Folding and unfolding of polymer helices in solution *Macromolecules* **40** 2559–67
[38] Cullis A G, Canham L T and Calcott P D J 1997 The structural and luminescence properties of porous silicon *Appl. Phys. Rev.* **82** 910–65
[39] Roe R 2000 *Methods of X-Ray and Neutron Scattering in Polymer Science* (New York: Oxford University Press)
[40] Wilcoxon J P, Samara G A and Provencio P N 1999 Optical and electronic properties of Si nanoclusters synthesized in inverse micelles *Phys. Rev.* B **60** 2704–14
[41] Sychugov I, Juhasz R, Valenta J and Linnros J 2005 Narrow luminescence linewidth of a silicon quantum dot *Phys. Rev. Lett.* **94** 087405
English D S, Pell L E, Zhonghua Y, Barbara P F and Korgel B A 2002 Size tunable visible luminescence from individual organic monolayer stabilized silicon nanocrystals quantum dots *Nano Lett.* **2** 681–5
[42] Cichos F, Martin J and Borczykowski C 2004 Emission intermittency in silicon nanocrystals *Phys. Rev.* B **70** 115314
[43] Fonseca L F, Resto O, Gupta S, Katiyar R S and Weisz S Z 1999 Optical properties and nanoparticle size distribution in luminescent porous silicon *Proc. 24th ICPS* ed D Gershoni (Singapore: World Scientific) pp 1–4